Nonuniversality in the Pinch-Off of Yield Stress Fluids: Role of Nonlocal Rheology

Louvet, N.; Bonn, D.; Kellay, H.

Link to publication

☙

Nonuniversality in the Pinch-Off of Yield Stress Fluids: Role of Nonlocal Rheology

Nicolas Louvet,[1,*] Daniel Bonn,[2] and Hamid Kellay[1]

[1]*Université de Bordeaux, Laboratoire Ondes et Matière d'Aquitaine, UMR 5798 U. Bx/CNRS,*
351 Cours de la Libération, 33405 Talence, France
[2]*Soft Matter Group, Van der Waals–Zeeman Institute, Institute of Physics, University of Amsterdam,*
Science Park 904, Amsterdam, Netherlands

The pinch-off behavior of yield stress fluids is investigated using droplet and liquid-bridge breakup experiments. Contrary to expectations, the neck thinning behavior depends strongly on the way the breakup experiment is carried out. This nonuniversal behavior can be explained through an analysis of the thinning dynamics as well as the shapes of the fluid necks. Recent nonlocal models for the rheology of yield stress fluids are found to be compatible with the results presented.

Yield stress fluids are used in many industrial processes such as fracturing, the pouring of concrete, and the preparation and packing of foodstuffs. These fluids behave as a solid when the applied stress is below the so-called critical yield stress but flow as a liquid above this threshold [1–3]. Flows encountered in practical situations can have a strong extensional component that cannot be described by commonly used shear constitutive laws. Recent theoretical work suggests a highly nontrivial link between shear and extensional behavior of jammed suspensions [4]. Since there is no constitutive equation describing yield stress materials in both shear and extension, measurements are needed.

We follow a simple and direct method to probe the extensional properties of a variety of yield stress fluids by following the capillary thinning dynamics of a fluid neck until it breaks up [5–7]. We find that, contrary to expectations, the thinning dynamics shows a nonuniversal behavior that leads to fluid viscosities that depend on the imposed initial deformation. While slow deformation experiments can be understood using the shear constitutive relation [8–11], the faster deformation data cannot be understood in a simple manner. Our results can be rationalized using recently introduced models for the nonlocal rheology of soft glassy materials [12–14].

We make use of two experimental setups, in order to address recent conflicting literature results on the breakup dynamics of yield stress fluids, raising questions as to what controls this dynamics [11,15]. The first experimental setup probes the breakup of a liquid bridge initially squeezed between two glass plates. The lower plate can be pulled vertically at a constant velocity V until the bridge breaks. V can be varied from 10^{-2} to 10^2 mm/s allowing us to significantly vary the initial imposed stretching rate. The initial bridge height and diameter are $L_0 \simeq 1$ mm and $D_0 \simeq 3$ mm, respectively. In the second setup, a drop is released from a capillary (inner diameter $D_0 = 4$ mm) at a

small flow rate so that the drop detaches only due to gravity. This configuration allows for the highest initial stretching rate. We use a camera fitted with a microscope objective lens to record the drop profile as a function of time at a frequency up to 30 kHz with a spatial resolution of 4 μm/pixel.

We use aqueous dispersions of Carbopol at a concentration of 2% and concentrated emulsions as ideal yield stress fluids [3,16]. Carbopol dispersions consist of individual elastic sponges with a diameter ranging from a few to tens of microns [3,16]. The emulsions are dispersions of castor oil droplets (volume fraction 74%) in 1% aqueous SDS solutions. The droplet size is 3.1 μm. The shear rheology of the dispersions is well described by the Herschel-Bulkley (HB) constitutive equation $\sigma = \sigma_{y,s} + k\dot{\gamma}^n$, where $\sigma_{y,s}$ is the shear yield stress, k the consistency parameter, and n the index of shear thinning [1]: $n = 0.4 \pm 0.03$ for the systems considered. The yield stress is 120 Pa for the dispersions and 10 Pa for the emulsions (see the Supplemental Material [17]). The measured extensional yield stress is roughly 1.6 times $\sigma_{y,s}$ (Supplemental Material [17]) in agreement with previous estimates [18] and theory of jammed suspensions of colloidal particles [4]. The surface tension and the density of the materials are $\gamma \simeq 50$ mN $\cdot$ m^{-1} and $\rho = 1000$ kg/m^3 for the dispersion and 18 mN/m and 980 kg/m^3 for the emulsion [15,19,20].

Photographs of the breakup are displayed in Fig. 1. While for low extension velocities the fluid neck has pronounced curvature in the lateral direction, the neck is much shallower for high velocities or for droplet pinch-off. In order to quantify such differences, Fig. 2 displays the minimum neck diameter $2h_{\min}$ versus time to breakup $\tau = (t_b - t)$. Theoretical work [8,9] and experiments [10,11,20] suggest that the thinning dynamics for so-called power-law shear-thinning fluids is universal and should follow $h_{\min} \propto \tau^n$. This result carries over to yield stress fluids obeying the HB equation as shown in Ref. [21] since
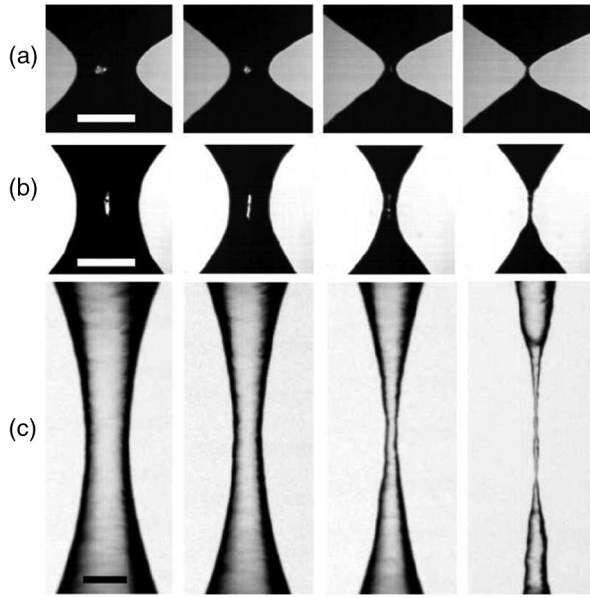
FIG. 1.   Liquid bridges and detaching drops of a 2% Carbopol solution at different extension velocities V and times to breakup τ: (a) $V = 0.018$ mm/s at $\tau = 3.59$, 1.2, 0.08, and 0.0001 s. (b) $V = 1.8$ mm/s at $\tau = 0.15$, 0.065, 0.0095, and 0.0001 s. (c) Droplet breakup at $\tau = 0.0067$, 0.0035, 0.0005, and 0.0001 s. The scale bar is 500 μm.

FIG. 2 (color online).   [(a),(b)] Minimum neck diameter $2h_{\min}(\tau)$ for different values of V. Fits are power laws with exponent n: The faster stretching rates have their time scale indicated on the upper axis (vertical arrow). [(c),(d)] η_s versus $\dot{\epsilon}_M$ for different V values along with the rheology. Fluids used: (a), (c), 2% Carbopol dispersion; (b), (d), 74% castor oil emulsion.

capillary stresses are generally higher than the critical yield stress so that they behave as power-law fluids. Recent experiments support this thinning law [10,11] by finding thinning dynamics to be well described by the exponent n; others do not [15] and find Newtonian behavior with a linear thinning law. Our system (Fig. 1) does not display a fracture modifying the thinning dynamics as reported in Refs. [22,23]. Furthermore, we conclude from our experiments that the thinning dynamics is sensitive to the way the breakup is produced. Figures 2(a) and 2(b) show that the thinning rates depend on initial conditions: the higher the velocity, the faster the thinning. This behavior is obtained for both the Carbopol dispersion and the castor oil emulsion. All curves in Figs. 2(a) and 2(b) can be fit with the power-law model but with values of n that depend on V. While the value of n is close to the one measured in shear flow for low velocities for either system as expected and observed [10,11], it increases towards a value of 1 for the droplet experiments as in Ref. [15]. This is our main result: the same fluid behaves differently depending on the imposed initial stretching rate, but the behavior remains that of a power-law fluid.

To illustrate this nonuniversality, we first extract the fluid viscosity from the thinning dynamics using $\eta_s = 2^{n-1} n^n \phi_0(n) \gamma [(dh_{\min})/(d\tau)]^{-1}$. Here, $\phi_0(n)$ is a constant; as tabulated in Ref. [9], its value for $n = 1$ matches the relation governing viscous fluid pinch-off, i.e., $\eta_s = 0.07 \gamma [(dh_{\min})/(d\tau)]^{-1}$ [6,24,25]. The prefactor $2^{n-1} n^n \phi_0(n)$ is discussed in the Supplemental Material
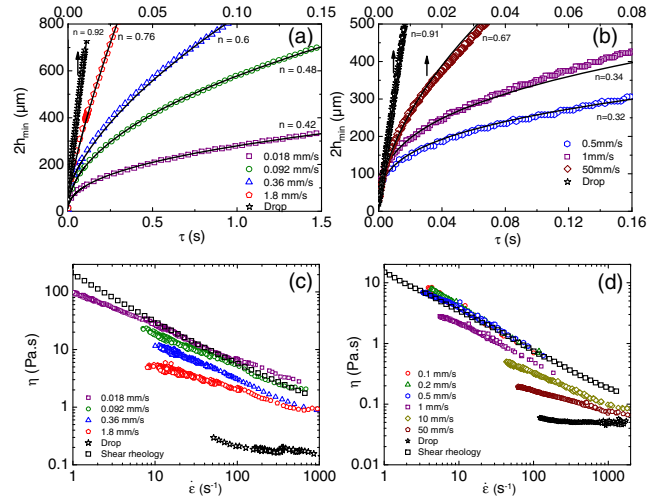
[17]. Figures 2(c) and 2(d) show viscosity (η_s) versus extension rate [$\dot{\epsilon}_M = (2/h_{\min})(dh_{\min}/d\tau)$]. The viscosity matches the shear rheology (obtained as $\sigma/\dot{\gamma}$) for low velocities as expected since the thinning dynamics follows the predicted behavior for a power-law fluid; the extensional rheology of the fluid follows the shear rheology, and the pinch-off behavior is due to a balance between viscous and capillary forces. For higher velocities and for the droplet, the viscosity is significantly lower and the power-law dependence of η_s versus $\dot{\epsilon}_M$ changes. Shear rheology and extensional rheology differ in this case.

Second, the spatial profiles of the fluid necks (interface position h versus vertical coordinate z) near the minimum neck location $z_{\min}$ are supposed to be similar for both Newtonian and power-law fluids [6,9]. A proper rescaling of $h(z)$ and z allows us to collapse the profiles for different τ onto a universal curve independent of initial conditions. The profiles are extracted from images as in Fig. 1 and rescaled according to the following form: $h(z)/h_{\min} = F[(z - z_{\min})/\tau^\delta]$; the normalization by τ^δ accounts for the scaling of the axial coordinate during thinning [9]. For the value of n considered here ($n = 0.4$), $\delta = 0.4$ [9]. We have used $h_{\min}^{\delta/n}$, which scales as τ^δ [9,10] to avoid uncertainty in the determination of the rupture time t_b. This rescaling is shown in Figs. 3(a) and 3(b) and gives $\delta \simeq 0.36$ for the lowest velocity. The function F is quadratic as shown by the solid lines leading to $h(z)/h_{\min} = C[(z - z_{\min})/h_{\min}^{\delta/n}]^2 + 1$ (C is a constant), which gives a good description of the data for both systems. The higher-velocity experiments require different values of n and δ. The value of n increases as V increases with δ, in reasonable agreement with predictions [9] as shown in the
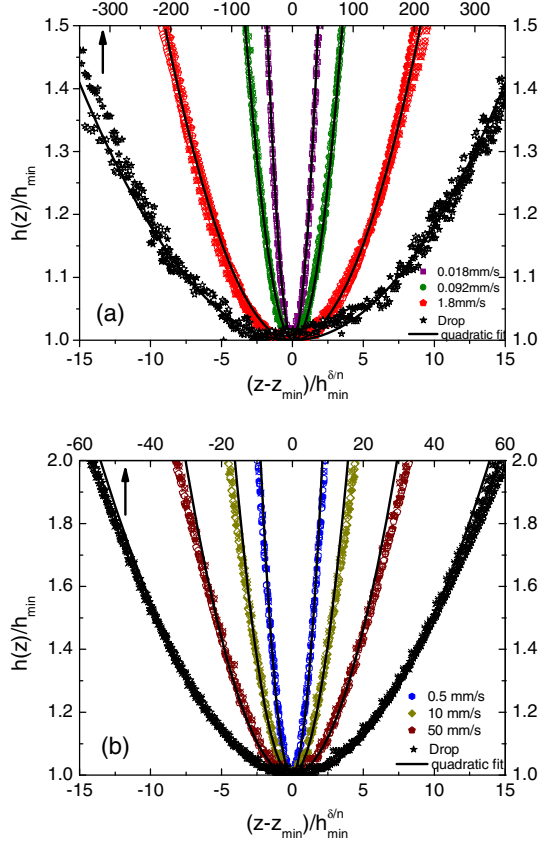
FIG. 3 (color online). Fluid bridge profiles (bottom axis) for different values of V and droplet profiles (top axis, indicated by arrows) for Carbopol dispersions (a) and castor oil emulsions (b). V ranges from 0.018 mm/s [red symbols in panel (a)] to 50 mm/s [brown symbols in panel (b)]. For each value of V and for the droplet curve, we probed four profiles, as indicated by four symbols (x, +, open, closed) in the same color. The corresponding values of h_{min} vary per profile but are typically between 35 and 500 μm. Solid lines are quadratic fits.

Supplemental Material [17]. The good agreement between expected behavior for power-law fluids and our experiments for the profiles and thinning dynamics supports us in neglecting inertia, elasticity, and normal stress effects [26]. Note that while profiles for each velocity can be collapsed onto a master curve, these master curves are different for each velocity due to the velocity dependence of n.

    Why do the profiles for different velocities differ, and why are the resulting viscosities so different from the shear rheology? In literature, experiments using dense suspensions showed that the viscosity in the final instants before breakup can be smaller than the expected viscosity and dilution effects have been invoked [27,28]. If dilution were at work, the local concentration of our suspensions would need to be decreased by a factor of 10 in these jammed suspensions of soft objects, which seems unlikely. Also, theoretical and numerical work give no hint as to possible changes of fluid behavior as observed here [21,29].

    A probable cause, as reported for the shear rheology of yield stress fluids in confined geometries, is the existence of a finite length scale over which the apparent viscosity of the fluid can be much smaller than the bulk viscosity [12–14]. This decrease is the result of local plastic events fluidizing the suspension over a cooperativity length scale ξ. This has been rationalized by defining [12] $\xi^2 \Delta f = f - f_b$, with fluidity f the inverse of the local viscosity, f_b the inverse of the bulk shear viscosity η_{shear}, and Δ the Laplacian operator (here, $\Delta f = [(\partial^2 f)/(\partial r^2)] + (1/r)(\partial f/\partial r) + [\partial^2 f/(\partial z^2)]$, r is in the radial direction and the azimuthal variation of f is neglected). For concentrated emulsions and for Carbopol dispersions, ξ is of the order of a few droplet or object sizes, respectively [12,14].

    To examine this model, we use the power-law fluid model to write the local viscosity as $\eta(z, \tau) = \beta[\dot{\epsilon}(z, \tau)]^{n-1}$, with β a constant. This viscosity depends on z since the local extension rate $\dot{\epsilon}(z, \tau) = [2/h(z, \tau)][dh(z, \tau)/d\tau]$ (Supplemental Material [17]) depends on z, reaching a maximum at z_{min} and decreasing away from it. Our estimate of η uses an $\dot{\epsilon}$ that is averaged over r, so our estimate of the fluidity denoted $\bar{f}$ is also an average over r: $\bar{f} = 1/\eta(z, \tau)$. As shown in Fig. 4(a), $\bar{f}$ goes through a maximum at $z = z_{min}$ and is much higher than f_b for the two examples shown and for all the runs we have carried out for the two
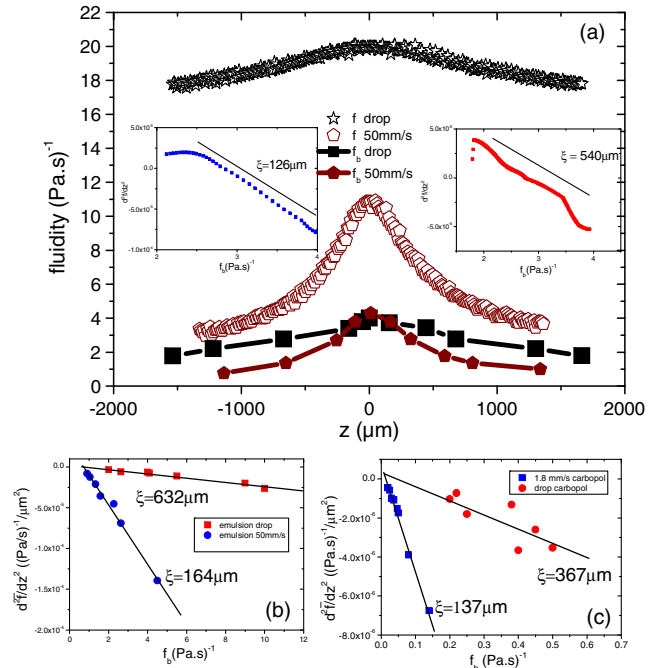

FIG. 4 (color online). (a) $\bar{f}$ and $\bar{f}_b$ profiles for the emulsion in two situations: a fluid bridge ($V = 50$ mm/s, $\tau = 0.0021$ s) and a droplet ($\tau = 0.0036$ s). Insets: $\partial^2 \bar{f}/\partial z^2$ versus $\bar{f}_b$ for the data of the main figure. (b) $\partial^2 \bar{f}/\partial z^2$ versus $\bar{f}_b$ evaluated at $z = z_{min}$ for an emulsion bridge ($V = 50$ mm/s) and droplet. (c) As in (b), for a dispersion bridge ($V = 1.8$ mm/s) and droplet.

systems. In the fluidity equation above, the right-hand side is positive while the left-hand side has a negative term, $\partial^2 f/\partial z^2$, since f goes through a maximum at $z = z_{min}$. This excludes using the fluidity model if f is independent of r, as the model would predict a viscosity that is larger than the bulk viscosity [30,31] in contradiction with our results.

One way to reconcile our results with the model is to introduce a variation of f in the direction r. In this case, f needs to go through a minimum versus r while it goes through a maximum versus z. Let us rewrite the fluidity equation averaged over r as $\partial^2 \bar{f}/\partial z^2 = [-\overline{(\partial^2 f/\partial r^2)} + \bar{f}/\xi^2] - f_b/\xi^2$ (Supplemental Material [17]). As the variation of f versus r cannot be obtained experimentally due to averaging over r, the fluidity equation can be tested only partially: as shown in the insets of Fig. 4(a), a linear relation is obtained between $\partial^2 \bar{f}/\partial z^2$ and f_b using the spatial fluidity profiles of Fig. 4(a) taken at a single instant. The equation can also be tested using data at different velocities and evaluating $\partial^2 \bar{f}/\partial z^2$ and f_b at $z = z_{min}$ at different times as shown in Figs. 4(b) and 4(c) for the two systems used and two different velocities. The linearity of the results can have two reasons. The first is that $[-\overline{\partial^2 f/\partial r^2} + \bar{f}/\xi^2]$ is proportional to f_b making it difficult to extract ξ without knowing the variation of f versus r. The second is that $\partial^2 f/\partial r^2 \simeq f/\xi^2$ giving $\partial^2 \bar{f}/\partial z^2 \simeq -(f_b/\xi^2)$. Under the latter assumption (Supplemental Material [17]), the value of ξ obtained from the slope of the linear variation (see Fig. 4) is roughly constant, independent of time for each experiment, and consistent with the values determined using the spatial profiles. ξ also increases as the velocity increases in agreement with the differences in behavior observed for the different rates. The order of magnitude of ξ is 100 μm, which is larger than the values obtained from shear flow experiments. The significance of these values and their variation with velocity remain to be understood in the absence of a model for the variation of f versus r. While our experiments cannot validate this variation, we can conclude it to be small: for the fluidity profiles in Fig. 4(a), the viscosity is at most 15% smaller at the surface than at the center of the neck (Supplemental Material [17]). A final point concerns the predicted variation of ξ close to yielding [12,13]. Within the precision of our experiments, no variation is observed here as in Ref. [12]. All these points merit further experiments with better precision and certainly further theoretical work to explore the significance of our findings and the limitations of the model.

In conclusion, we studied the extensional flow of yield stress fluids in liquid-bridge breakup experiments. The bridge thinning is very sensitive to the initial conditions, leading to nonuniversal thinning dynamics, which cannot be rationalized by a simple shear constitutive law. Upon extension, the fluid behaves as a power-law fluid with an exponent depending on the initial stretching rate. We have examined whether nonlocal effects can describe the strong deviations from bulk rheology. While the analysis of our data using this phenomenology is only partial, it suggests two things. First, the cooperativity length depends on the applied stretching rate: the higher the stretching rate, the larger the cooperativity length and, hence, the larger the deviations from bulk rheology. Second, the viscosity at the neck needs to vary, albeit mildly, in the radial direction, giving a nontrivial neck structure which remains to be tested. The nonlocal rheology model therefore gives rise to nontrivial consequences whose significance remains to be fully understood to validate the model or point to its possible limitations.

*Present address: Laboratoire d'Energétique et de Mécanique Théorique et Appliquée (LEMTA), Université de Lorraine-CNRS, UMR 7563, F-54504 Vandoeuvre-Lès-Nancy, France.

[1] H. Herschel and R. Bulkley, Proc., Am. Soc. Test. Mater. **26**, 621 (1926).

[2] Q. D. Nguyen and D. V. Boger, Annu. Rev. Fluid Mech. **24**, 47 (1992); H. A. Barnes, J. Non-Newtonian Fluid Mech. **81**, 133 (1999); D. Bonn and M. M. Denn, Science **324**, 1401 (2009).

[3] G. Ovarlez, S. Cohen-Addad, K. Krishan, J. Goyon, and P. Coussot, J. Non-Newtonian Fluid Mech. **193**, 68 (2013).

[4] J. M. Brader, M. E. Cates, and M. Fuchs, Phys. Rev. Lett. **101**, 138301 (2008).

[5] G. H. McKinley, Annu. Rheol. Rev. **1** (2005); G. H. McKinley and T. Sridhar, Annu. Rev. Fluid Mech. **34**, 375 (2002).

[6] J. Eggers, Rev. Mod. Phys. **69**, 865 (1997); J. Eggers and E. Villermaux, Rep. Prog. Phys. **71**, 036601 (2008).

[7] F. Ingremeau and H. Kellay, Phys. Rev. X, **3**, 041002 (2013).

[8] M. Renardy, J. Non-Newtonian Fluid Mech. **103**, 261 (2002); M. Renardy and Y. Renardy, J. Non-Newtonian Fluid Mech. **122**, 303 (2004).

[9] P. Doshi, R Suryo, O. E. Yildirim, G. H. McKinley, and O. A. Basaran, J. Non-Newtonian Fluid Mech. **113**, 1 (2003); P. Doshi and O. A. Basaran, Phys. Fluids **16**, 585 (2004); R. Suryo and O. A. Basaran, J. Non-Newtonian Fluid Mech. **138**, 134 (2006).

[10] J. R. Savage *et al.*, Soft Matter **6**, 811 (2009).

[11] F. M. Huisman, S. R. Friedman, and P. Taborek, Soft Matter **8**, 6767 (2012).

[12] L. Bocquet, A. Colin, and A. Ajdari, Phys. Rev. Lett. **103,** 036001 (2009); J. Goyon, A. Colin, G. Ovarlez, A. Ajdari, and L. Bocquet, Nature (London) **454,** 84 (2008); J. Goyon, A. Colin, and L. Bocquet, Soft Matter **6,** 2668 (2010).

[13] A. Nicolas and J. L. Barrat, Phys. Rev. Lett. **110,** 138304 (2013).

[14] P. Jop, V. Mansard, P. Chaudhuri, L. Bocquet, and A. Colin, Phys. Rev. Lett. **108,** 148301 (2012).

[15] M. Aytouna, J. Paredes, N. Shahidzadeh-Bonn, Sébastien Moulinet, C. Wagner, Y. Amarouchene, J. Eggers, and D. Bonn, Phys. Rev. Lett. **110,** 034501 (2013).

[16] J. M. Piau, J. Non-Newtonian Fluid Mech. **144,** 1 (2007).

[17] See the Supplemental Material at http://link.aps.org/ supplemental/10.1103/PhysRevLett.113.218302 for the results of the extensional yield stress measurements, the stress shear rate measurements, the characteristics of the thinning, and information about the fluidity model and its applicability.

[18] L. Martinie, H. Buggisch, and N. Willenbacher, J. Rheol. **57,** 627 (2013); K. Niedzwiedz, H. Buggish, and N. Willenbacher, Rheol. Acta **49,** 1103 (2010).

[19] J. Boujlel and P. Coussot, Soft Matter **9,** 5898 (2013).

[20] A. L. Yarin, E. Zussman, and A. Theron, J. Rheol. **48,** 101 (2004).

[21] N. J. Balmforth, N. Dubash, and A. C. Slim, J. Non-Newtonian Fluid Mech. **165,** 1139 (2010).

[22] M. I. Smith, R. Besseling, M. E. Cates, and V. Bertola , Nat. Commun. **1,** 114 (2010).

[23] C. Ligoure and S. Mora, Rheol. Acta **52,** 91 (2013).

[24] D. T. Papageorgiou, Phys. Fluids **7,** 1529 (1995).

[25] A. Rothert, R. Richter, and I. Rehberg, Phys. Rev. Lett. **87,** 084501 (2001).

[26] Normal stress effects are negligible since the shear rates in the neck region are negligible. The effects of elasticity can be gauged through the so-called Deborah number De $= \dot{\epsilon}(k/G)^{1/n}$ [32]. As the elastic modulus G is about 900 Pa for Carbopol and 100 Pa for the emulsion, De is close to 1 for the highest $\dot{\epsilon}$ (1000 s^{-1}). Consequently, De is smaller than 1 for most of the data. If we consider the initial stretching rates used, De does not exceed 0.1 for the highest initial stretching rates used. Inertial effects may also play a role in droplet pinch-off. An estimate of the Reynolds number Re $\sim (R_0/l_\nu)^{1/2}$ [6] where R_0 is the capillary radius or the initial radius of the neck and l_ν is the viscous length scale defined as $(\eta^2/\rho\gamma)$ where η is the shear viscosity of the fluid gives for initial times Re of the order of 10^{-5} for Carbopol and 10^{-3} for the emulsion. At high extension rates, Re is of order 0.1 for Carbopol and 1 for the emulsion in the worst-case scenario.

[27] C. Bonnoit, T. Bertrand, E. Clément, and A. Lindner, Phys. Fluids **24,** 043304 (2012).

[28] M. Roché, H. Kellay, and H. A. Stone, Phys. Rev. Lett. **107,** 134503 (2011).

[29] P. Coussot and F. Gaulard, Phys. Rev. E **72,** 031409 (2005).

[30] P. Chaudhuri, V. Mansard, A. Colin, and L. Bocquet, Phys. Rev. Lett. **109,** 036001 (2012).

[31] V. Mansard, A. Colin, P. Chaudhuri, and L. Bocquet, Soft Matter **9,** 7489 (2013).

[32] L.-H. Luu and Y. Forterre, J. Fluid Mech. **632,** 301 (2009).